Black carbon modelling in urban areas: investigating the influence of resuspension and non-exhaust emissions in streets using the Street-in-Grid model for inert particles (SinG-inert)

Lya Lugon[1,2], Jérémy Vigneron[3], Christophe Debert[3], Olivier Chrétien[2], and Karine Sartelet[1]

[1]CEREA, École des Ponts ParisTech, EDF R&D, 77455 Champs-sur-Marne, France
[2]Paris City, Departement of green spaces and environment, 103 Avenue de France, France
[3]Airparif, France

Correspondence: Lya Lugon (lya.lugon@enpc.fr), Karine Sartelet (karine.sartelet@enpc.fr)

Abstract.

Black carbon (BC) is a primary and inert pollutant often used as a traffic tracer. Even though its concentrations are generally low at regional scale, BC presents very high concentrations in streets (local scale), potentially causing important effects on human health and environment. Modelling studies of BC concentrations usually underestimate BC concentrations, because of uncertainties in both emissions and modelling. Both exhaust and non-exhaust traffic emissions present uncertainties, but those on non-exhaust emissions, such as tyre, brake and road wear and particle resuspension, are particularly high. In terms of modelling, the street models do not always consider the two-way interactions between the local and regional scales. With the two-way modeling approach, a street with high BC concentrations may influence urban background concentrations above that street, which can finally enhance the BC concentrations in the same street. This study uses the multi-scale Street-in-Grid model (SinG) to simulate BC concentrations in a Paris suburb street-network, taking into account the two-way coupling between local and regional scales. The BC concentrations in streets proved to have an important influence on urban background concentrations. The two-way dynamic coupling leads to an increase in BC concentrations in large streets with high traffic emissions (with a maximal increase of about 48%), and a decrease in narrow streets with low traffic emissions and low BC concentrations (with a maximal decrease of about 50%).

A new approach to estimate particle resuspension in streets is implemented, strictly respecting the mass balance on the street surface. The resuspension rate is calculated from the available deposited mass on the street surface, which is estimated based on a particle deposition and wash-off parametrizations adapted to street-canyon geometries. The simulations show that particle resuspension presents a low contribution to black carbon concentrations, as the deposited mass is not significant enough to justify high resuspension rates.

Non-exhaust emissions, such as brake and tyre and road wear, may largely contribute to BC emissions, with a contribution equivalent to exhaust emissions. Here, a sensitivity analysis of BC concentrations is performed by comparing simulations with different emission factors of tyre, brake and road wear. The different emission factors considered are estimated based on the literature. We found a satisfying model-to-measurement comparison using high tyre-wear emission factors, which may indicate that tyre-emission factors usually used in Europe are probably under-estimated. These results have important policy

25 implications: public policies replacing internal-combustion engines by electric vehicles may not eliminate BC air pollution, but only reduce it by half.

1 Introduction

Black carbon (BC) is a primary and chemically inert atmospheric pollutant, compound of $PM_{2.5}$ (particulate matter of diameter lower than 2.5 μm). BC background concentrations in urban areas are generally quite low, but they can reach high values in
30 streets. The Parisian air-quality agency (AIRPARIF) performed a chemical speciation of particulate matter between September 2009 and September 2010. They found that BC concentration represented approximately 4% of $PM_{2.5}$ concentrations in rural areas, 10% in urban background, reaching 27% in a street with high traffic (AIRPARIF, 2012). BC is mainly emitted by traffic, and then it is often used as a traffic pollutant tracer (Invernizzi et al., 2011; de Miranda et al., 2019). During winter the wood burning in residential heating is also an important source of BC in some regions, such as Paris city (AIRPARIF, 2012). A
35 special attention is given to BC because of its potential impacts on human health. Recent studies showed a strong correlation between BC concentrations and the occurrence of cancers (Lequy et al., 2021), respiratory and cardiovascular problems (Jansen et al., 2005; Highwood and Kinnersley, 2006; Janssen et al., 2011; Dons et al., 2012), and also impacts on fetus development (Zhang et al., 2019a, b). BC is also responsible for environmental impacts due to its radiative properties (light absorption), which lead to visibility reduction (Tao et al., 2009; Chen et al., 2016; Li et al., 2019)(Tao et al., 2009; Chen et al., 2016; Li
40 et al., 2019) and global warming (Jacobson, 2001; Chung and Seinfeld, 2005; Tripathi et al., 2005; Ramachandran and Kedia, 2010).

Although BC concentration is high in urban streets, BC concentration and its dispersion are often not modelled at the street scale. Most of air-quality studies regarding BC employ statistical regression techniques, that estimate BC concentrations over a street network based on meteorological data and punctual observations (Richmond-Bryant et al., 2009; Awad et al.,
45 2017; Van den Bossche et al., 2018; Sanchez et al., 2018; Van den Hove et al., 2019; Boniardi et al., 2019; Liu et al., 2019; Jones et al., 2020). When street or street-network models are used, emission data are often modified and/or are coupled to observational data to improve modelled concentrations. For example, Brasseur et al. (2015) used a street model over two street canyons in Brussels. To achieve the high BC concentrations observed in the streets, a correction factor of 3.0 was applied to traffic emissions calculated with COPERT IV, a database that provides traffic emissions factors for European vehicles
50 (Ntziachristos and Samaras, 2018). This under-estimation is also suggested in studies using more complex local-scale models for BC dispersion. For example, Tong et al. (2011) simulated BC concentrations using the Comprehensive Turbulent Aerosol Dynamics and Gas Chemistry (CTAG) in an urban region at South Bronx, New York. A good correlation between observed and simulated BC concentrations was reached combining field measurements and numerical simulations and increasing by 15% the number of heavy-duty diesel vehicles in the morning peaks (and consequently increasing BC emissions). The corrections
55 applied to BC emissions in these studies suggest an under-estimation of BC emissions.

Uncertainties in BC concentrations modelled with street-network models are partly due to uncertainties in traffic emissions. Traffic emissions are classified as exhaust emissions, and non-exhaust emissions, from tyre, brake and road wear and particle

resuspension. On one hand, exhaust emissions are relatively well-known, as they are characterized in laboratory controlled conditions. In Europe, exhaust emission factors are nowadays determined according to the vehicle technology and fuel, providing realistic emission factors for divers vehicle fleet. The details about vehicle categories, technologies and fuel are detailed in the EMEP guidelines (Ntziachristos and Samaras, 2018). However, Ntziachristos and Samaras (2018) also provide information about BC emissions, by providing a speciation of $PM_{2.5}$ in the form of $BC/PM_{2.5}$ ratios. They vary depending on the vehicle category (light-duty vehicles LDV or heavy-duty vehicles HDV), fuel and regulatory standard of the vehicle manufacturing (Euro norm), as presented in Table 3.91 of Ntziachristos and Samaras (2018). The uncertainties of the $BC/PM_{2.5}$ ratios depend on the vehicle category. For LDV diesel vehicles, which present the highest $BC/PM_{2.5}$ ratios, the uncertainties of $BC/PM_{2.5}$ ratios are quite low, ranging from 5 to 10%. For diesel vehicles equipped with particle filter, the uncertainties are high (about 50%), but with a lower $BC/PM_{2.5}$ ratio than other diesel vehicles, and also with a lower $PM_{2.5}$ emission rate.

On the other hand, non-exhaust emissions are still not well-known in the literature, and they are not included in regulatory emissions legislation. Non-exhaust emissions consist of particles emitted from vehicles operation and linked to tyre, brake and road wear and resuspension. Their emission factors are greatly variable and associated to large uncertainties. Uncertainties in non-exhaust emissions can be explained by the difficulty to dissociate emissions from the different processes and by the great variability of: (i) tyre, brake and road constituents used in different locations; (ii) vehicles characteristics, such as weight, location of driving wheels, etc; (iii) vehicles operational conditions, such as vehicles speed and ambient temperature; and (iv) methodologies to determinate wear emission factors, i.e. direct measurements *in-situ*, with wind-tunnel experiments or receptor-oriented methods (Boulter, 2005; Thorpe and Harrison, 2008). These uncertainties are reflected in the estimation of the contribution of non-exhaust emissions to PM concentration observed in the literature, as detailed in Section 2.

Another aspect that may affect the under-estimation of BC concentrations in simulations is the one-way coupling approach usually employed in street-network or local-scale models. Street-network models often use prescribed background concentrations. Although the vertical mass transfer between the streets and the background influenced the concentrations in the streets, its influence on the background concentrations is often neglected. The multi-scale model Street-in-Grid (SinG) combines the Model of Urban Network of Intersecting Canyons and Highways (MUNICH) (Lugon et al., 2020; Kim et al., 2018) for modelling street concentrations and Polaid3D for modelling background concentrations (Sartelet et al., 2007), allowing to simulate local and regional scale simultaneously. SinG performs a two-way coupling between regional and local scales, taking into account at each iteration the influence of the vertical mass transfer between the background and the streets on both the background and the street concentrations. This two-way coupling between the streets and the background can be especially important for BC, as the concentrations observed in streets are considerably larger than BC concentrations in the urban background. Previous studies regarding gas-phase pollutants observed an important effect of the two-way coupling on NO_2, NO and NO_x concentrations in the streets, which may reach 60% in streets with high traffic emissions (Lugon et al., 2020; Kim et al., 2018).

This study presents simulations of BC concentrations in a Parisian suburb street-netwok using the model SinG. It investigates the influence of non-exhaust emissions on BC concentrations in the streets, presenting a sensitivity analysis of wear emission factors, and a new approach to estimate particle resuspension respecting mass conservation on the street surface. It also investigates the importance of a two-way coupling between regional and local scales, by comparing BC

concentrations in streets calculated by SinG and MUNICH as a stand-alone model (MUNICH-only). Emission factors of tyre, brake and road wear are calculated based on the literature and sensitivity tests are performed. Model to data comparisons are based on BC observations performed during the TRAFIPOLLU campaign (https://trimis.ec.europa.eu/project/multiscale-modeling-traffic-pollutants-urban-area), in a street called "Boulevard Alsace Lorraine". The same measurement site was already used by Kim et al. (2018) for the evaluation of NOx and NO_2 concentrations simulated by SinG. Section 3 describes SinG, emphasizing the parametrizations of particles deposition, wash-off and resuspension. Section 4 summarizes simulations setup, at both regional and local scales. Section 5 describes the sensitivity analysis to estimate the importance of tyre, brake and road-wear emissions on BC concentrations, and section 6 presents the influence of the two-way coupling between the regional and local scales on BC concentrations in the streets.

2 Uncertainties and variability of emissions factors observed in non-exhaust emissions

As mentioned in the introduction, non-exhaust emissions still present high uncertainties, and a great variability of emission factors is observed the literature. This section presents an overview of the different studies that estimate particle non-exhaust emissions. It also includes some studies that investigate their BC content.

According to Berdowski et al. (2002), non-exhaust emissions contribute to only 3.1% of PM_{10} and 1.7% of $PM_{2.5}$ concentrations in European countries, and specifically in France to 2.2% of PM_{10} and 1.1% of $PM_{2.5}$. Similarly, Dore et al. (2003) estimated that the contribution of non-exhaust emissions is low: they estimated that 80% of inhalable PM are emitted from road traffic, of which only 3% are non-exhaust emissions. Differently, other studies estimated that the contribution of non-exhaust emissions is very high. Rauterberg-Wulff (1999) obtained tyre wear emission factors using wind-tunnel experiments in controlled conditions of the same order of magnitude than diesel exhaust emissions. Using tunnel measurement techniques, Lawrence et al. (2016) quantified PM_{10} emission factors from exhaust and non-exhaust sources for a vehicle fleet. They estimated non-exhaust PM_{10} emission factor to be 50% higher than the exhaust emission factor: 49% of PM_{10} emissions were estimated to be non-exhaust emissions, 33% to be exhaust emissions and 18% were considered as unexplained emissions. Brake and road wear presented an important contribution to PM_{10} emissions, with almost the same emission factor as petrol exhaust. Resuspension process had the higher emission factor (10.4 mg.(veh-km)-1 against 4.5 mg.(veh-km)-1 of petrol exhaust and 8.3 mg.(veh-km)-1 of diesel exhaust), followed by unexplained sources (7.2 mg.(veh-km)-1). Harrison et al. (2001) measured PM_{10} and $PM_{2.5}$ at five sites in the United Kingdom in order to perform a correlation between emission sources and PM_{10} concentrations. They estimated that the mass of coarse particles ($PM_{10-2.5}$) from non-exhaust emissions is approximately the same as the mass of fine particles ($PM_{2.5}$) from exhaust emissions. Note that important differences are observed in their size distribution. Exhaust emissions are composed of tiny particles, with diameters lower than 1 μm (Ntziachristos and Samaras, 2018). Particles from non-exhaust emissions are coarser. According to the European Emission guidelines (Ntziachristos and Boulter, 2016), 60% of particles emitted from tyre wear are PM_{10}, 42% are $PM_{2.5}$, and only 6% are PM_1. Particles from brake-wear emissions have lower diameters: 98% are PM_{10}, 39% are $PM_{2.5}$, and 10% are PM_1. The coarsest particles are those from road wear: 50% are PM_{10}, 27% are $PM_{2.5}$, and there is no PM_1. The non-exhaust emissions can also be very important for

secondary particle formation, especially regarding secondary organic aerosol (SOA). Khare et al. (2020) highlighted the importance of asphalt-related emissions in SOA formation, still absent from emission inventories. These emissions are dependent of the solar radiation and temperature over the asphalt surface, and are variable according to the asphalt life cycle stages (such as storage, paving, and use). The annual estimation of asphalt-related SOA precursor emissions at urban scales is estimated to
130 exceed those from motor vehicles. These studies show that non-exhaust emissions can be very important for air-quality, and that it is necessary to improve the identification source techniques and the parametrizations to quantify non-exhaust emission rates.

A few emission models try to integrate vehicle operational conditions to estimate non-exhaust emission factors, based on empirical factors and simplified parameterizations (Guevara et al., 2020; Denby et al., 2013a). The High-Elective Resolution
135 Modelling Emission System (HERMES) model Guevara et al. (2020) employs the non-exhaust emission factors proposed in the EMEP guidelines (Ntziachristos and Boulter, 2016), which provide PM_{10} wear emission rates for passenger cars, motorcycles, LDV and HDV. A speed correction ratio is adopted for tyre and brake wear emission factors, ranging from 1.39 and 0.902 for tyre wear and 1.67 and 0.185 for brake wear. Specifically for HDV, PM_{10} tyre and brake-wear emissions are calculated taking into account vehicle weight, represented by a load factor ranging from 0 to 1. HDV tyre-wear emissions also take into account
140 the vehicle size by the number of axles. A detailed description of non-exhaust emission factors employed in the HERMES model is available in the EMEP guidelines (Ntziachristos and Boulter, 2016), and a brief summary is presented in section 4.2 of this paper. PM_{10} emission rates from tyre, brake and road wear indicated in the EMEP guidelines are quite low. Tyre wear emission rates are around 6 mg.(veh-km)-1 for LDV, and 18 mg.(veh-km)-1 for HDV, brake wear emission rates are around 8 mg.(veh-km)-1 for LDV, and 40 mg.(veh-km)-1 for HDV, and road wear emission rates equal to 7.5 mg.(veh-km)-1 for LDV
145 and 38 mg.(veh-km)-1 for HDV. Differently, the NORTRIP model takes into account the vehicle speed to determine PM_{10} tyre and road wear emission rates, but not for brake-wear emissions, which are assumed to be independent of vehicle speed. The NORTRIP model adopts a linear regression based on tyre and road wear emission rates observed at a reference speed of 70 km.h^{-1}. Road-wear emissions also take into account the road characteristics, as the pavement hardness. A detailed description of non-exhaust emission factors employed in the NORTRIP model is available in Denby et al. (2013a). Quite similar tyre and
150 brake wear rates are obtained using the EMEP guidelines and the NORTRIP model. The road-wear emissions calculated using the NORTRIP model with the road characteristics employed by Thouron et al. (2018) in "Boulevard Alsace Lorraine" (a street East of Paris). They are higher than those proposed in the EMEP guidelines, by a ratio 6.0, because of their different algorithm and road characteristics. More details about tyre, brake and road-wear emissions using the NORTRIP model and the EMEP guidelines emission factors are presented in section 5.
155 Other studies assume constant non-exhaust emission factors for separate sources, and they show a great variability of several orders of magnitude between emission factors for tyre wear. The bibliographic review presented in Boulter (2005) shows different tyre wear emission factors, ranging from 10 mg.(veh-km)-1 to 100000 mg.(veh-km)-1. Tyre wear emission factor of the order of 100 mg.(veh-km)-1 for passenger cars are observed in the literature: Luhana et al. (2004) measured an average tyre wear emission rate for passenger cars of 97 mg.(veh-km)-1, and Baumann and Ismeier (1997) of 80 mg.(veh-km)-1.
160 According to the bibliographic review presented in the US Environmental Agency (EPA) report (available at https://cfpub.epa.

gov/si/si_public_file_download.cfm?p_download_id=525701, Table 3-1), other studies proposed tyre-wear emissions rates for LDV around 100 mg.(veh-km)−1, such as Gebbe (1997) (110 mg.(veh-km)−1), and Malmqvist (1983) (120 mg.(veh-km)−1). Higher LDV tyre wear rates, around 200 mg.(veh-km)−1, were estimated by Councell et al. (2004) and Baekken (1993), and 300 mg.(veh-km)−1 by Schuring and Clark (1988) (ranging from 240 mg.(veh-km)−1 to 360 mg.(veh-km)−1). Tyre wear emission rates could be even higher according to the ambient and operational conditions: Park et al. (2018) investigated tyre wear particles generated in a laboratory under different tyre/road contact conditions and observed important variations in tyre wear emission factors and size distributions with the variation of road cornering conditions. At constant speed conditions (80 km.h^{-1}), the tyre wear emission rates obtained with a 2° tyre slip angle were about 300 times larger than those obtained with no tyre slip angle, increasing from 3.5 mg.km^{-1} to 1110.8 mg.km^{-1} per tyre. Considering a vehicle with 4 tyres, the tyre-wear emissions range from 14 mg.(veh-km)−1 to 4443.2 mg.(veh-km)−1 only with a 2° tyre slip angle variation.

Brake-wear emissions present a lower variability, according to the literature. The greater variations in PM$_{10}$ brake wear emission are observed by Abu-Allaban et al. (2003) using a receptor modelling technique, ranging from 0 to 80 mg.(veh-km)−1 for LDV and 0 to 610 mg.(veh-km)−1 for HDV. Other experimental studies estimate lower brake wear emission rates, with typical values around 8 mg.(veh-km)−1 for LDV and 40 mg.(veh-km)−1 (Grigoratos and Martini, 2015; Denby et al., 2013a; Sanders et al., 2003; Ntziachristos and Boulter, 2016).

Road emission factors vary from 3.8 mg.vkm^{-1} (Boulter, 2005) to 200 mg.vkm^{-1} (Thouron et al., 2018). Compared to other non-exhaust emission sources, road-wear emission factors present the worst quality codes, according to the European emission guidelines EMEP (Ntziachristos and Boulter, 2016), where different quality codes are defined for non-exhaust emissions, ranging from B (emission factors non statistically significant based on a small set of measured re-evaluated data), C (emission factors estimated on the basis of available literature), to D (emission factors estimated applying similarity considerations and/or extrapolation). Road wear is the emission source with the worst quality code, and they highlight the difficulties to separate precisely the non-exhaust emission sources and the dependence of road characteristics and vehicles operational conditions.

Among the non-exhaust emissions, particle resuspension is probably the process that presents the largest uncertainties. Divers studies estimate resuspension emission factors, often higher than exhaust emissions but with a variability of several orders of magnitude. Luhana et al. (2004) observed relatively low resuspension factors: about 0.8 mg.(veh-km)−1 for LDV and 14.4 mg.(veh-km)−1 for HDV. Note that the same study observed an important contribution of tyre wear, with an average emission factor of 94 mg.(veh-km)−1 for passenger cars. Lawrence et al. (2016) determined the emission factors from for a typical vehicles fleet (composed of 92% of passenger cars) with wind-tunnel experiments. Resuspension presented the higher emission factor (10.4 mg.(veh-km)−1), in contrast with lower emission factors from combustion (4.5 mg.(veh-km)−1 for gasoline vehicles and 8.3 mg.(veh-km)−1 for diesel vehicles), tyre and brake wear (4.4 mg.(veh-km)−1), road wear (4.5 mg.(veh-km)−1), and unexplained sources (7.2 mg.(veh-km)−1). For a similar fleet, Pay et al. (2011) measured PM$_{10}$ resuspension factors in Berlin, and estimated them to be 88 mg.(veh-km)−1 for LDV and 217 mg.(veh-km)−1 for HDV. These values were adopted in the the HERMES model to calculate particles resuspension in Spain (Pay et al., 2011) and led to a similar impact on PM$_{10}$ concentrations as exhaust emissions. Note that other non-exhaust emission factors used in the HERMES model are based on the EMEP guidelines, but no resuspension emission rate is defined by Ntziachristos and Boulter (2016)

due to the great uncertainties observed in the literature. In the HERMES model, resuspension emission factors are the most important non-exhaust emission source, and no precision about vehicle operational conditions and the available mass in surface are considered. Other studies obtained even higher resuspension factors: 10-1000 mg.(veh-km)−1 (Venkatram et al., 1999), 7600-8400 mg.(veh-km)−1 (Moosmüller et al., 1998), 40-780 mg.(veh-km)−1 for LDV and 230-7800 mg.(veh-km)−1 for HDV (Abu-Allaban et al., 2003), showing the huge uncertainties in particle resuspension factors.

Considerable difficulties to differentiate tyre, brake and road-wear emissions from resuspension are mentioned in experimental studies (Thorpe et al., 2007; Ntziachristos and Boulter, 2016; Beji et al., 2020), which indicate that these wear emissions factors may be even higher than expected and with different possible classification among sources. Due these difficulties, Beji et al. (2020) classified non-exhaust emissions as brake-wear emissions and tyre-road contact particles, grouping tyre and road wear and resuspension in the same source.

Resuspension emission factors can be employed in air-quality models (Pay et al., 2011), but besides the uncertainties in these emission factors, the methodology does not necessarily respect mass balance on the street surface. If resuspension is implemented in the model using resuspension emission factors, a mass balance between total particle emissions, deposition, drainage caused by rain (wash-off) and resuspension factors may not hold. However, this mass balance may be used to determine the available particle mass on the street surface that may be resuspended. The NORTRIP model (Denby et al., 2013a, b) computes particle resuspension based on a street surface mass balance, also integrating the particle wash-off. But the NORTRIP model artificially assumes that tyre, brake and road-wear emissions are instantly deposited over the street surface, and only these sources are employed to calculate the particle mass on the street.

Beyond the uncertainties attached to PM non-exhaust emission factors, their chemical composition is still not well-known. Tyre-wear emissions contain a large fraction of BC, as BC represents 22%-30% of tyre weight (Thorpe and Harrison, 2008). Quite similarly, the BC fraction observed in tyre-wear emitted particles, is about 13%-19% (Kreider et al., 2010), 18% (Park et al., 2017), and 15.3% (Ntziachristos and Boulter, 2016). Road and brake wear present lower BC fractions, with 1.06% (± 50%) and 2.6% respectively according to Ntziachristos and Boulter (2016). More recently Lyu and Olofsson (2020) investigated BC emissions from disc brakes, and concluded that the BC fraction in PM_1 emitted from brake wear is higher than the BC fraction from combustion process. The BC fractions observed in PM_1 emitted by three different types of brake ranged from 20.7% to 72.4%, with an average value of 41.5%, depending on the surface conditions and graphite content of the brake materials. These studies regarding non-exhaust emission characteristics emphasize that the knowledge on the BC emissions from tyre, brake and road wear is far from complete, and further studies are required.

3 Model description

Street-in-Grid (SinG) is a multi-scale model that performs a dynamic two-way coupling between the street-network model MUNICH (Model of Urban Network of Intersecting Canyons and Highways) and the 3D chemistry-transport model Polair3D. As detailed in Lugon et al. (2020), this dynamic coupling between local and regional scales allows a direct interaction between concentrations in the street network and those in the urban background: the mass transfer between the street and the background

concentrations influence both the street and the background concentrations. Furthermore, SinG uses consistent chemical and physical parameterizations, such as the same chemical module and meteorological data, at both local and regional scales. Note that the street-network model MUNICH can also be used as a stand-alone model, with a one-way coupling approach. In this case the background concentrations influence the concentrations in the streets, but the mass transfer between streets and the background do not influence background concentrations. SinG and MUNICH are described in Lugon et al. (2020) and Kim et al. (2018), and Polair3D is presented by Boutahar et al. (2004); Sartelet et al. (2007), all available in the Polyphemus platform (Mallet et al., 2007). The size distribution of BC is modeled with a sectional approach, with diameters ranging typically from 10^{-3} μm and 10 μm. Because BC is an inert species, this study does not take into account chemical reactions, and only BC concentrations are modelled. The aerosol dynamics (nucleation, coagulation and condensation/evaporation) is also neglected, as it would have no effect on BC mass concentration and low effect on size distribution.

Particle resuspension is the non-exhaust emission process that presents the largest uncertainty and variability. Different studies in the literature propose constant resuspension emission factors (see section 1), but this methodology does not necessarily respect mass conservation on the street surface. This study presents a new methodology to calculate particle resuspension, based on the respect of mass conservation on the street surface. At each time iteration, SinG calculates the total particle mass available on the street surface (M_{dep}), taking into account particle deposition (Q_{dep}), wash-off (Q_{wash}) and resuspension (Q_{res}) rates, by integrating the following equation:

$$\frac{dM_{dep}}{dt}\bigg|_{surf} = Q_{dep} - (Q_{wash} + Q_{res}). \tag{1}$$

As detailed in section 3.3, the parametrizations used to calculate particle resuspension are based on the NORTRIP model (Denby et al., 2013a), but with an important difference: NORTRIP calculates the deposited mass assuming that all wear emissions are directly deposited, and deposition is not directly linked to the concentrations of particles in the street. Here, the concentrations of particles are computed with SinG, as detailed in Lugon et al. (2020), and particle deposition is computed from the concentrations, meaning that the time to deposit is taken into account (no instantaneous deposit), and particles from all origins (e.g. exhaust, non exhaust, particles transported from other sources) may deposit. The formulations used for deposition, washout and resuspension in the street surface mass balance equation are now detailed.

3.1 Particle deposition

Particle and gas dry-deposition modelling follows the Cherin et al. (2015) approach, designed for street canyons. This parametrization calculates separately particle deposition over the different available surfaces in a street canyon, such as pavement area and building walls. Note that only the particle deposition on the street pavement is considered when computing the street-surface deposited mass, which is available for resuspension. A complete description of this approach is detailed in Cherin et al. (2015), with the computation of deposition velocities for gas and particulate species. The deposition mass rate Q_{dep} is proportional to the deposition velocity v_{dep} and the species concentration in the street C_{sp}. Particle deposition velocities varies with particle

260   diameter, indicated by the size section b:

$$Q_{dep} = v_{dep,b} \times C_{sp,b}. \tag{2}$$

3.2   Particle wash-off

Particle wash-off over the street surface is computed using the concept of wash-off factor f_{wash}, as described in Denby et al. (2013a, b). In this parametrization, the particle mass rate drained by water Q_{wash} is proportional to f_{wash} and the deposited

265   mass over the surface M_{dep}, as detailed in Equations (3) and (4):

$$f_{wash} = \frac{1}{\delta t} \left(1 - exp \left(-h_{drain,eff} \frac{g_{road} - g_{road,min}}{g_{road,min}} \right) \right), \tag{3}$$

$$Q_{wash} = f_{wash} \times M_{dep}, \tag{4}$$

with δ_t the time step between two evaluations of g_{road} (600 s here), $h_{drain,eff}$ the drainage efficiency parameter, g_{road} the amount of water presents on the street surface [mm], $g_{road,min}$ the minimum water content to drainage process [mm].

270   Note that the drainage efficiency $h_{drain,eff}$ depends on particle properties. It can range from 0 to 1, depending on the species mixing state and solubility. As discussed in Denby et al. (2013a) and Vaze and Chiew (2002), salt should be well mixed and very soluble in water, thus having high drainage efficiency. Because dust and BC are insoluble species, and because they may not be well mixed with salts (Zhu et al., 2016; Majdi et al., 2020), their drainage efficiency should be poor. Here, $h_{drain,eff}$ is taken equal to 0.001, as proposed in Denby et al. (2013b); g_{road} corresponds to the water rain calculated in each street and

275   integrated in time from the meteorology, and $g_{road,min}$ is 0.5 mm, as in Denby et al. (2013b). Drainage is treated in the model as an instantaneous process, as performed by Denby et al. (2013a) and Denby et al. (2013b).

3.3   Particle resuspension

Particle resuspension is calculated based on a resuspension factor f_{res}, as proposed by Denby et al. (2013a) and employed in the NORTRIP model. This factor varies depending on the traffic flow characteristics, such as the LDV and HDV vehicle flow

280   and speed:

$$f_{res} = \sum_{v=1}^{2} N_v \left(\frac{u_v}{u_{ref(r)}} \right) f_{0,v}, \tag{5}$$

where v indicates the vehicle type, N_v the vehicle flow [veh.h^{-1}], u_v the vehicle speed [km.h^{-1}], $u_{ref(r)}$ is the reference vehicle speed for the resuspension process [km.h^{-1}], and $f_{0,v}$ the reference mass fraction of the resuspension process [veh^{-1}]. As used in (Denby et al., 2013a) and Thouron et al. (2018), this study adopts $u_{ref(r)} = 50$ km.h^{-1}, $f_{0,hdv} = 5 \times 10^{-5}$ veh^{-1}

285   and $f_{0,ldv} = 5 \times 10^{-6}$ veh^{-1}.

The resuspension rate Q_{res} is then calculated as detailed in Equation (6), as a function of the deposited mass on the street surface M_{dep} [μg]:

$$Q_{res} = f_{res} \times M_{dep}. \tag{6}$$

3.4 Solving particle mass balance over the street surface

Using the formulations of wash-off and resuspension presented in Equations (4) and (6), the time evolution of the surface mass (Equation (1)) can be rewritten as:

$$\left. \frac{dM_{dep}}{dt} \right|_{surf} = Q_{dep} - M_{dep}(f_{wash} + f_{res}), \tag{7}$$

with an analytical solution:

$$M_{dep(t)} = \begin{cases} \frac{Q_{dep}}{(f_{wash}+f_{res})} + \left(M_{dep(t-1)} - \frac{Q_{dep}}{(f_{wash}+f_{res})} \right) \times exp(-(f_{wash} + f_{res})\delta t) \text{ if } (f_{wash} + f_{res}) \neq 0, \\ M_{dep(t-1)} + Q_{dep} \times \delta t \text{ if } (f_{wash} + f_{res}) = 0. \end{cases} \tag{8}$$

As indicated in the previous sections, M_{dep} is determinant to calculate the particle resuspension and wash-off. It represents the maximal particle mass that can be resuspended, to ensure mass conservation on the street surface. Besides the respect of mass conservation on the street surface, this approach presents other advantages: (i) particle deposition is estimated from concentrations (and not from wear emissions as in NORTRIP), following a formulation adapted to street-network geometries, and (ii) no additional hypothesis is necessary to determine chemical speciation of resuspended particles, as resuspended and deposited particles are assumed to have the same composition. A limitation of this approach lies in the difficulty to estimate the resuspension factor f_{res} and its variations with chemical species.

To compute the concentrations in the street volume, MUNICH and SinG solves an equation describing the time evolution of the mass M in each street segment (Kim et al., 2018; Lugon et al., 2020). New terms are added to this equation: the particle resuspension rate Q_{res}; the tyre, brake and road emission rates ($Q_{emis,wear}$) as an inlet flux, and the particle wash-off rate Q_{wash} as an outlet flux. They are highlighted in Equation (9), which is solved for each size section:

$$\left. \frac{dM}{dt} \right|_{volume} = \underbrace{(Q_{inflow} + Q_{emis,exh} + \mathbf{Q_{res}} + \mathbf{Q_{emis,wear}})}_{inlet \; flux} - \underbrace{(Q_{outflow} + Q_{vert} + Q_{dep,v} + \mathbf{Q_{wash}})}_{outlet \; flux}, \tag{9}$$

with $Q_{emis,exh}$ the exhaust traffic emission rate, Q_{inflow} the mass inflow rate at intersections, Q_{vert} the turbulent mass flux between the atmosphere and the street, $Q_{outflow}$ the outflow flux, and $Q_{dep,v}$ the deposition flux over the street volume v, considering the street pavement and building walls surfaces. These terms are detailed in Kim et al. (2018) and Lugon et al. (2020). Concentrations calculated in each street using Equation (9) are then used to compute the deposition mass flux, as mentioned in Section 3.1.

4 Simulations setup

This section describes the input data and the model configuration of the SinG simulations, at both the regional and local scales. Six particle size sections are employed, with bound diameters 0.01, 0.0398, 0.1585, 0.4, 1.0, 2.5 and 10 μm. Simulations were run from 15 March to 15 May 2014. Model to data comparisons are performed from 12 April to 15 May, where BC concentrations were measured at the air monitoring station operated by Airparif during the TRAFIPOLLU project (https://anr.fr/Projet-ANR-12-VBDU-0002).

4.1 Regional scale

SinG is employed to simulate BC concentrations over a regional-scale domain covering Paris with a spatial resolution of 1 km x 1 km (domain 4), as illustrated in Figure 1. Initial and boundary concentrations are obtained from nested simulations at the regional scale using the model Polair3D, over Europe (domain 1, spatial resolution of 55 km x 55 km), France (domain 2, spatial resolution of 11 km x 11 km), Île-de-France region (domain 3, spatial resolution of 2 km x 2 km) and Greater Paris (domain 4, spatial resolution of 1 km x 1 km). All four domains have the same vertical discretization with 14 levels, from 0 to 12 km. Meteorological data are calculated using the WRF model (version 3.9.1.1), as detailed in Lugon et al. (2020).
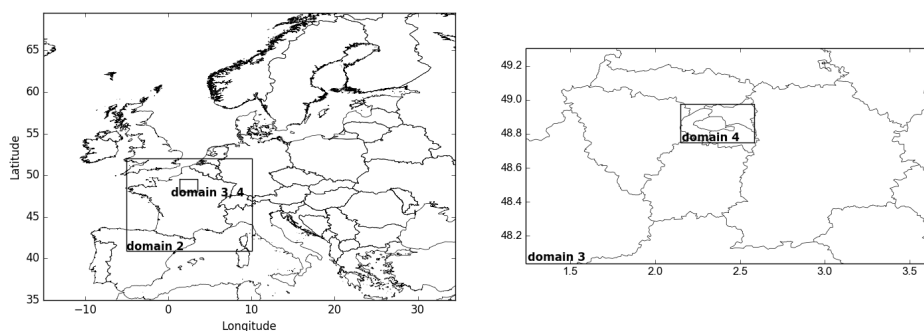
Figure 1. Regional-scale nested domains: Europe (domain 1, spatial resolution 55 km x 55 km), France (domain 2, spatial resolution 11 km x 11 km), Île de France region (domain 3, spatial resolution 2 km x 2 km) and Greater Paris (domain 4, spatial resolution 1 km x 1 km).

BC emissions over Europe (domain 1) and France (domain 2) are obtained from the European Monitoring and Evaluation Program (EMEP) emission inventory for the year 2014, with a spatial resolution of 0.1° x 0.1°.

Over the Île-de-France region (domain 3) and Greater Paris (domain 4), sources other than traffic are obtained using the AIRPARIF emission inventory of 2012. Because the simulated period corresponds to spring/summer in France with low contribution of the residential sector, the differences between the emissions of 2012 and 2014 for sectors other than traffic have a low impact on BC modelling over Paris. BC traffic emissions are computed using the emission inventory of 2014 provided by the air-quality agency of Paris (AIRPARIF), except in the street-network region (see Figure 2), where they are obtained from the TRAFIPOLLU project, as detailed in the section "Local scale" below. For BC traffic non-exhaust emissions, over domain

4 (both in the street-network region and outside), different scenarios of non-exhaust emissions are studied, as described in the section 5 (see Table 1).

335   Note that in SinG, which is used over domain 4, traffic emissions are not used for the regional-scale modelling in the street-network region, but only for the local-scale (street) modelling, because the local and regional scales are two-way coupled.

4.2   Local scale

At the local scale, SinG simulates the street network represented in Figure 2, containing 577 streets including the "Boulevard Alsace Lorraine", where the measurements were performed. Meteorological data above each street are extracted from the same
340 WRF simulation as employed at the regional scale.
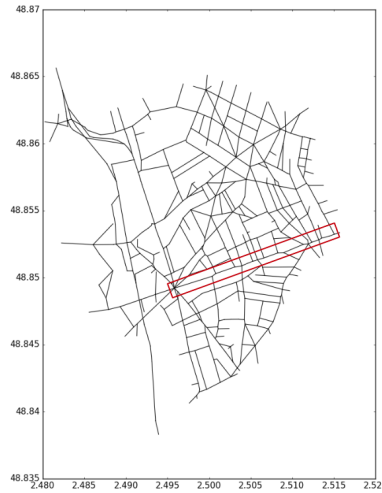
Figure 2. The street network, with the "Boulevard Alsace Lorraine" highlighted in the red rectangle.

    BC exhaust traffic emissions are obtained from the TRAFIPOLLU project, using the same street network and exhaust inventory as detailed in Kim et al. (2018): the dynamic traffic model SymuVia was used to determine the hourly traffic in each street of the network and pollutant emissions were deduced using COPERT IV emissions factors; emissions were calculated for two typical days: 25 March 2014, representative of weekdays, and 30 March 2014, representative of a week-ends and holidays.
345 BC non-exhaust emission factors from tyre, brake and road wear are computed using the formulations proposed in the EMEP guidelines (Ntziachristos and Boulter, 2016) to calculate PM_{10} wear emissions, and a speciation represented by a BC fraction (f_s^{bc}), defined for each wear source. The values used in this study for $EF_{s,v}^{tsp}$, $f_s^{pm_{10}}$ and f_s^{bc} are detailed in section 5.

$$EF_{s,v}^{bc} = EF_{s,v}^{tsp} \times f_s^{pm_{10}} \times S_s(u_v) \times f_s^{bc}. \tag{10}$$

where s is the non-exhaust source (tyre, brake or road wear, indicated by ty, bk and rd respectively), v is the vehicle type (v = LDV or HDV), $EF_{s,v}^{tsp}$ is the total suspended particles (TSP) wear emission rate for a determined source s and vehicle v, f_s^{pm10} the PM$_{10}$ fraction of TSP emitted by each wear source s and S_s the correction factor according to vehicle speed u_v. S_s varies according to the wear emission source, as shown in Equations (11), (12) and (13):

$$S_{ty}(u_v) = \begin{cases} 1.39 \text{ if } u_v < 40\text{km.h}^{-1}, \\ -0.00974u_v + 1.78 \text{ if } 40\text{km.h}^{-1} \leq u_v \leq 90\text{km.h}^{-1}, \\ 0.902 \text{ if } u_v > 90\text{km.h}^{-1}, \end{cases} \tag{11}$$

$$S_{bk}(u_v) = \begin{cases} 1.67 \text{ if } u_v < 40\text{km.h}^{-1}, \\ -0.0270u_v + 2.75 \text{ if } 40\text{km.h}^{-1} \leq u_v \leq 95\text{km.h}^{-1}, \\ 0.185 \text{ if } u_v > 95\text{km.h}^{-1}, \end{cases} \tag{12}$$

$$S_{rd}(u_v) = 1.0. \tag{13}$$

The total suspended particles wear rates emitted by tyre and brake wear in HDV ($EF_{s,hdv}^{tsp}$) are computed as a function of passenger cars (PC) wear emissions. They take into account the vehicle characteristics as HDV weight (represented by a load correction factor LCF_s) and the number of axles (N_{axle}), as indicated in Equations (14) and (15).

$$EF_{ty,hdv}^{tsp} = \frac{N_{axle}}{2} \times LCF_s \times EF_{ty,pc}^{tsp}, \tag{14}$$

$$EF_{bk,hdv}^{tsp} = 3.13 LCF_s \times EF_{bk,pc}^{tsp}, \tag{15}$$

with LCF_s a load correction computed as a function of the load factor LF, ranging from 0 and 1.

$$LCF_s = \begin{cases} 1.41 + (1.38 LF) \text{ for tyre wear }, \\ 1.00 + (0.79 LF) \text{ for brake wear }. \end{cases} \tag{16}$$

The resulting non-exhaust emission rate ($Q_{emis,wear}$) for all wear emission source s is proportional to the LDV and HDV vehicle flow (N_v), as indicated in Equation (17):

$$Q_{emis,wear} = \sum_{s=1}^{3} \sum_{v=1}^{2} \left(EF_{s,v}^{bc} \times N_v \right). \tag{17}$$

As particle resuspension is directly dependent on the particle mass deposited on the street surface, it is dependent on the initial conditions of the simulation. In order to avoid this dependence, a spin up of 25 days is adopted to enable a mass surface equilibrium between deposition, wash-off and resuspension mass rates. More details are provided in section 5.3.

5 Sensitivity analysis to black carbon non-exhaust emissions

370 As mentioned in the introduction, non-exhaust emissions are difficult to estimate. The huge variability of car models and speed regimes, combined to a large diversity of tyre, brake and road components contribute to the large uncertainties associated to non-exhaust emissions. Furthermore, experimental studies report the complexity to differentiate resuspension from tyre and road-wear emissions.

This section presents a sensitivity analysis of BC street concentrations to BC non-exhaust emissions, using different tyre, 375 brake and road emission factors from the literature.

5.1 The simulations

Different simulations were performed using SinG, with large variations in tyre-wear emissions properties. The BC fractions adopted in brake and road wear are constant in all simulations and they are the same in all emitted size sections. They follow the EMEP guidelines (Ntziachristos and Boulter, 2016) with $f_{bk}^{bc} = 0.026$ and $f_{rd}^{bc} = 0.0106$. Table 1 summarises the configuration 380 used in each simulation, with the PM_{10} fraction employed in each source s ($f_s^{pm_{10}}$), the BC fraction adopted in tyre-wear emissions (f_{ty}^{bc}), and the resultant BC emission factor from each vehicle type v (LDV and HDV) and non-exhaust source s ($EF_{v,s}^{bc}$).

To show the influence of non-exhaust emissions, simulation 1 ignores non-exhaust emissions. Simulation 2 employs the BC wear emission factors and size distribution indicated in the EMEP guidelines, also used in the HERMES model (Guevara 385 et al., 2020; Ntziachristos and Boulter, 2016). TSP tyre wear emission factors from HDV vehicles $EF_{hdv,ty}^{tsp}$ are deduced from Equations (14), considering a load factor LF equals to 1.0, and a number of axles N_{axle} equals to 2.0. Simulation 3 uses the PM_{10} wear emission factors and size distribution indicated in the NORTRIP model (Denby et al., 2013a). They are of the same order of magnitude than those of the EMEP guidelines. Note that for road-wear emissions, the road characteristics used in Bouvelard Alsace Lorraine by Thouron et al. (2018) were employed, leading to higher road-wear emissions than in the EMEP 390 guidelines. As NORTRIP does not indicate the BC fractions from each source, the same BC fractions as in the EMEP guidelines (Ntziachristos and Boulter, 2016) are adopted. Simulation 4 employs the same brake and road-wear emission factors as in the EMEP guidelines, but tyre-wear emission factors are higher. The same size distribution of non-exhaust emissions indicated in the EMEP guidelines (Ntziachristos and Boulter, 2016) is employed. A LDV tyre emission factor $EF_{ldv,ty}^{tsp}$ of 100 mg.(veh-km)-1 is used, as proposed in several studies Malmqvist (1983); Baumann and Ismeier (1997); Gebbe (1997); Luhana et al. 395 (2004); Boulter (2005). As in simulation 2, the TSP tyre-wear emission factors from HDV vehicles $EF_{hdv,ty}^{tsp}$ are deduced from Equations (14), considering a load factor LF equals to 1.0, and a number of axles N_{axle} equals to 2.0. A PM_{10} fraction $f_{ty}^{pm_{10}}$ 0.6 is adopted, as in simulation 2. More details about particle size distribution of non-exhaust emissions are indicated in Table A2, in the Appendix A3.

The tyre-wear BC fraction f_{ty}^{bc} is higher than in simulations 2 and 3. It is taken equal to 0.25, which is the average of the 400 BC mass weight fraction in tyre compositions (between 22%-30%) indicated in Thorpe and Harrison (2008). As in the EMEP guidelines and simulation 2, a speed correction factor $S_{ty}(u_v)$ of 1.39 is employed in the simulation, as the LDV and HDV

vehicle speed in the street network are lower than 40 km.h^{-1} (average speed around 32 km.h^{-1} according to TRAFIPOLLU measurements). The resulting PM$_{10}$ and BC tyre-wear emission factors from LDV and HDV are then EF$^{pm_{10}}_{ldv,ty}$ = 83.4 mg.(veh-km)−1, EF$^{pm_{10}}_{hdv,ty}$ = 232.7 mg.(veh-km)−1, EF$^{bc}_{ldv,ty}$ = 20.8 mg.(veh-km)−1 and EF$^{bc}_{hdv,ty}$ = 57.1 mg.(veh-km)−1.

405   In order to evaluate the impact of particle resuspension on BC concentrations in streets, simulation 5 uses the same setting of simulation 4, but it does not take into account particle deposition, and then, particle resuspension is not computed. This simulation physically represents the concentrations obtained with a maximal BC resuspension, which is equal to the BC deposition. Finally, in order to evaluate the influence of uncertainties in the BC speciation of exhaust emissions, simulation 6 uses the same non-exhaust emission factors as simulation 4, but BC exhaust emissions are artificially increased by 23%. This correc-

410   tion factor is defined using a linear correlation based on (i) the traffic-flow characteristics observed in the "Boulevard Alsace Lorraine" during the TRAFIPOLLU campaign (percentage of diesel and petrol vehicles, according to the vehicle category and technology), and (ii) the BC/PM$_{2.5}$ uncertainties for each vehicle class detailed in Table 3-91 of Ntziachristos and Samaras (2018).

Table 1. List of the simulations performed, with the configuration options (with or without deposition, with or without exhaust emission correction), the PM$_{10}$ fraction (f^{pm10}_s) adopted in each wear emission source (tyre wear indicated by ty, brake wear indicated by bk, and road wear indicated by rd), the BC fraction adopted in tyre-wear emissions (f^{bc}_{ty}), and the correspondent BC emission factors for each wear-emission source and vehicle type hdv and ldv (EF$^{bc}_{v,s}$) in mg.(veh-km)−1.

Sim.[1]	with dep.	with exh. emis. cor.	$f^{pm_{10}}_{ty}$	f^{bc}_{ty}	EF$^{bc}_{ldv,ty}$	EF$^{bc}_{hdv,ty}$	$f^{pm_{10}}_{bk}$	EF$^{bc}_{ldv,bk}$	EF$^{bc}_{hdv,bk}$	$f^{pm_{10}}_{rd}$	EF$^{bc}_{ldv,rd}$	EF$^{bc}_{hdv,rd}$
1	yes	no	0.00	0.00	0.00	0.00	0.00	0.00	0.00	0.00	0.00	0.00
2	yes	no	0.60	0.153	1.36	3.81	0.98	0.32	1.79	0.50	0.08	0.40
3	yes	no	0.10	0.153	0.71	3.58	0.80	0.21	1.04	0.18	0.47	2.40
4	yes	no	0.60	0.250	20.8	57.1	0.98	0.32	1.79	0.50	0.08	0.40
5	no	no	0.60	0.250	20.8	57.1	0.98	0.32	1.79	0.50	0.08	0.40
6	yes	yes	0.60	0.250	20.8	57.1	0.98	0.32	1.79	0.50	0.08	0.40

5.2   Model to measurement comparisons

415   The different simulations are evaluated by model to measurement comparisons of BC concentrations, measured at "Boulevard Alsace Lorraine". The statistical criteria applied to evaluate the model performance are those defined by Hanna and Chang (2012) and Herring and Huq (2018). Two different criteria are defined, (i) a lest strict criteria, accepted in urban areas, with

[1]1 - only exhaust emissions (Ntziachristos and Samaras, 2018); 2 - exhaust emissions (Ntziachristos and Samaras, 2018) and non-exhaust wear emissions from Ntziachristos and Boulter (2016); 3 - exhaust emissions (Ntziachristos and Samaras, 2018) and non-exhaust wear emissions based on Denby et al. (2013a); 4, 5 and 6 exhaust emissions (Ntziachristos and Samaras, 2018) and non-exhaust wear emissions based on Boulter (2005).

-0.67 < FB < 0.67; NMSE < 6; FAC2 ≥ 0.3; NAD < 0.5, and (ii) a most strict criteria, with -0.3 < FB < 0.3; 0.7 < MG < 1.3; NMSE < 3; VG < 1.6; FAC2 ≥ 0.5; NAD < 0.3 [2]. The definitions of the statistical indicators are given in Annex A1.

420   Table 2 shows the statistical indicators obtained from the model to measurement comparisons for each simulation of Table 1. The BC concentrations observed at "Boulevard Alsace Lorraine" are strongly underestimated in simulations 1, 2 and 3, with a fractional bias (FB) equal to -1.26, -1.10 and -1.15 respectively. They do not satisfy any performance criterion, nor the less strict ones, except for normalised mean square error (NMSE). However, the configurations used in simulations 4, 5 and 6, with higher tyre-wear emissions, result in satisfactory statistical indicators. They respect both the less and most strict performance criteria

425   proposed by Hanna and Chang (2012) and Herring and Huq (2018). The temporal evolution of BC concentrations obtained with simulation 4 is illustrated in Figure 3, showing a good correlation between the BC hourly concentrations observed and those simulated by SinG. Both the NORTRIP and the HERMES models, whose emission factors are used in simulations 1, 2 and 3, have quite low PM_{10} tyre-wear emission factors compared to the simulations 4, 5 and 6, which use higher tyre-wear emission factor for passenger cars, as proposed in the review Boulter (2005). The simulations performed by Pay et al. (2011)

430   and Denby et al. (2013a), using HERMES and NORTRIP models respectively, achieved good correlations between simulated and measured particle concentrations. They assume that resuspension is the main non-exhaust emission process, using high resuspension rates and relatively low tyre-wear emission factors. The PM_{10} resuspension rates used by Pay et al. (2011) (88 mg.(veh-km)−1 for LDV and 217 mg.(veh-km)−1 for HDV) are similar to the tyre-wear emission factors employed in simulations 4, 5 and 6 (83.4 mg.(veh-km)−1 for LDV and 232.7 mg.(veh-km)−1 for HDV). These high resuspension rates may

435   compensate the low non-exhaust tyre-wear emissions employed in the HERMES and NORTRIP models. The ratio between the total BC emissions in simulation 4 and simulation 2 is 3.30. A quite similar ratio of 3.0 was employed by Brasseur et al. (2015) to increase BC emissions from COPERT-IV emission inventory, as mentioned in the introduction.

Table 2. Comparisons to BC measurements at "Boulevard Alsace-Lorraine": statistical indicators obtained for the different SinG simulations.

	o [μg.m^{-3}]	s [μg.m^{-3}]	FB	MG	NMSE	VG	FAC2	NAD
1	6.07	1.37	-1.26	0.22	3.69	11.62	0.04	0.63
2	6.07	1.74	-1.10	0.29	2.54	5.80	0.12	0.55
3	6.07	1.62	-1.15	0.27	2.85	6.97	0.09	0.58
4	6.07	4.91	-0.21	0.82	0.29	1.27	0.77	0.19
5	6.07	4.92	-0.20	0.82	0.29	1.27	0.77	0.19
6	6.07	5.12	-0.16	0.85	0.27	1.26	0.78	0.18

The comparison between simulations 4 and 5 shows that particle dry-deposition has a low impact on BC concentrations in the streets (0.15% on average). Because the BC mass that may be resuspended is limited by the BC deposited mass, this

440   means that BC resuspension is also not significant compared to the other BC emission sources. Figure 5 illustrates the temporal evolution of BC deposition, wash-off and resuspension. The resuspension rate is limited by the deposited mass at the surface,

---

[2]FB represents the fractional bias, MG the geometric mean bias, NMSE the normalised mean square error, VG the geometric variance, NAD the normalised absolute difference, and FAC2 the fraction of predictions within a factor two of observations.
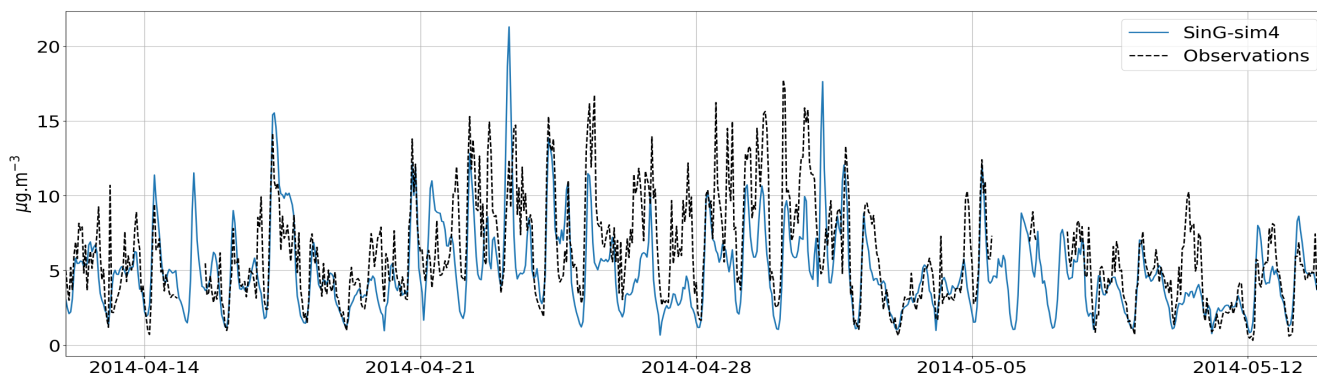
Figure 3. BC hourly concentrations at "Boulevard Alsace Lorraine" simulated by SinG (simulation 4) and observed in the TRAFIPOLLU campaign [μg.m^{-3}].

and both resuspension and deposition rates are of the same order of magnitude. BC wash-off mass rates present the same order of magnitude of reposition and resuspension processes, and are concentrated in raining days. This finding of low resuspension rate agrees with the observation of Luhana et al. (2004), which estimate that tyre-wear emissions are the most important 445 non-exhaust emissions, and that particle resuspension is not very important.
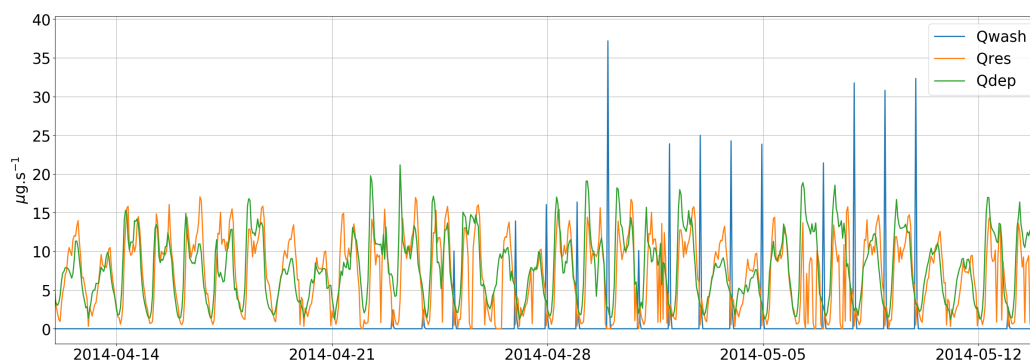
Figure 4. BC wash-off, deposition and resuspension rates simulated by SinG (simulation 4) [μg.s^{-1}].

The comparison between simulations 4 and 6 shows that increasing BC exhaust emissions by taking into account the uncertainties of the BC speciation in exhaust emissions lightly improves the BC concentrations in streets. Differences in BC concentrations simulated by modifying the BC exhaust emissions are less important than the differences simulated by modifying the BC tyre-wear emissions, suggesting that non-exhaust emissions are the most crucial emissions to improve.

5.3 Deposited mass over streets

A good representation of the particle deposited mass over the street surface is determinant to calculate the particle resuspension. This section compares the simulated particle deposited mass over the " Alsace Lorraine" to the one observed by Hong et al. (2016a) during the TRAFIPOLLU campaign. Hong et al. (2016a) collected *in-situ* the total road dust with dry sampling by a vacuum cleaner on 14 October 2014 at different points of the avenue. Figure 8a of Hong et al. (2016a) indicates the estimated total weight of dry stocks (in kg), ranging from 1 to 21 kg and with an average value about 8.90 kg. Considering the road surface is 2661 m^2, as indicated in Hong et al. (2016a), the TSP mass density in "Boulevard Alsace Lorraine" is 3.34 g.m^{-2}. The size distribution of these samples is presented in Figure 5 of Hong et al. (2016b), indicating that approximately 7.5% of the total deposited mass is composed of particles of diameters lower than 10 μm (PM$_{10}$). Therefore, the average mass density of PM$_{10}$ in "Boulevard Alsace Lorraine" is about 250 mg.m^{-2}. Note that quite similar PM$_{10}$ mass density was observed by Amato et al. (2009) in Barcelona urban areas (ranging from 8.9 to 216 mg.m^{-2}). In the simulations, to deduce the PM$_{10}$ deposited mass from the BC deposited mass, the fraction of BC in the PM$_{10}$ deposited mass at the surface is assumed to be 2.11%, following the observations of the chemical patterns of PM$_{10}$ in deposited road dust in urban environment performed by Amato et al. (2009).

Figure 5 illustrates the PM$_{10}$ deposited mass density (in mg.m^{-2}) obtained with each simulation at "Boulevard Alsace Lorraine". As mentioned in section 4.2, a spin-up of 25 days is used in each simulation, so that the deposited mass is independent of the initial conditions. Hence, here model to measurement comparisons are performed starting from 12 April. In Figure 5, this initial time of model to measurement comparisons (12 April) is indicated by the black vertical line. This spin-up is important to avoid an underestimation of particle deposition due to initial conditions. Table 3 summarizes the average PM$_{10}$ mass density obtained from 12 April to 14 May in all simulations, the PM$_{10}$ mass density estimated using the measurements performed by Hong et al. (2016a, b), and the corresponding FB between these mass densities. A good model to data correspondence is observed for simulations 4 and 6 with FB = -0.16 and -0.06 respectively. In simulations 1, 2 and 3, the particle deposited mass at the street surface is strongly underestimated, with a FB around -0.60. Note that simulation 5 does not consider particle deposition, so no particle deposited mass is present at the street surface.

Table 3. Average mass density of PM$_{10}$ deduced from the measurements at "Boulevard Alsace Lorraine" (obs. PM$_{10}$) [mg.m^{-2}], average simulated mass density of PM$_{10}$ (sim PM$_{10}$) [mg.m^{-2}], and the fractional bias (FB) [.].

	obs PM$_{10}$	sim PM$_{10}$	FB
sim-1	250	125.9	-0.66
sim-2	250	145.3	-0.53
sim-3	250	132.0	-0.62
sim-4	250	212.3	-0.16
sim-5	250	0.0	-2.00
sim-6	250	234.1	-0.06
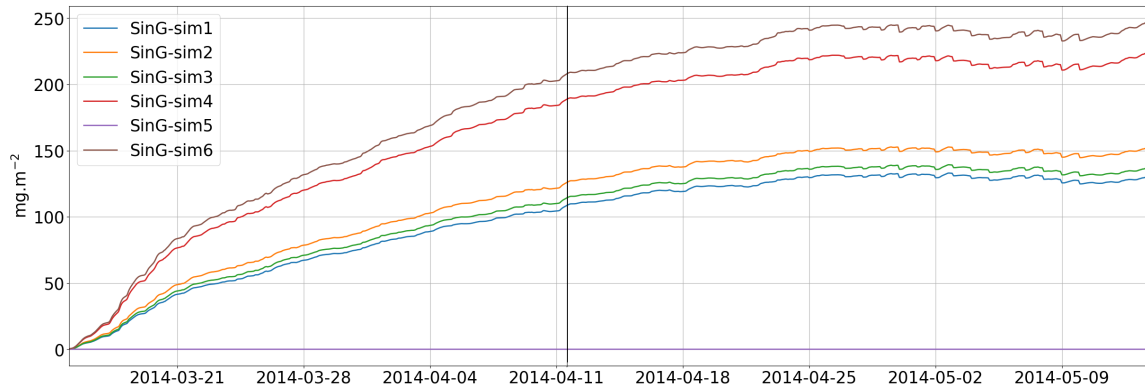
Figure 5. Temporal evolution of equivalent PM_{10} deposited mass density over the "Boulevard Alsace Lorraine" surface obtained with the different SinG simulations (in $mg.m^{-2}$).

6 Influence of the two-way coupling on BC concentrations in streets

This section investigates the influence of the two-way coupling between the regional and local scales on BC concentrations in the street network. For this, the concentrations calculated by SinG, with the two-way approach, are compared with those calculated by MUNICH as a stand-alone model, with the one-way approach. As mentioned in section 3, the coupling between the local and regional scales is two way in SinG, which couple the street model MUNICH to the chemistry transport model Polair3D. However, MUNICH may be used as a standalone model, simulating the street concentrations with a one-way coupling to the regional-scale background concentrations. In that case, the regional-scale (background) concentrations influence the street concentrations, but the street concentrations do not influence the background concentrations, and the vertical mass transfer between local and regional scales only influences concentrations in the streets. Note that in the one-way coupling, traffic emissions are used both in the regional-scale model Polair3D and in the street model MUNICH. Because SinG employs a two-way coupling, at each time step the vertical mass transfer between local and regional scales enables to calculate concentrations in the background and in streets, providing a direct interaction between concentrations in the street network and those in the urban background. Therefore, traffic emissions are considered only at the local scale, and there is no double counting of traffic emissions in SinG.

Simulations of BC concentrations using Polair3D, MUNICH and SinG are performed using the non-exhaust emission factors of simulation 4 (see Table 1). Regarding specifically the BC concentrations at the Boulevard Alsace Lorraine, both SinG and MUNICH as a stand-alone model (MUNICH-only) resulted in similar concentrations, respecting the most strict performance criteria (see Table A1 in Appendix A2). However, the differences between MUNICH and SinG depend on the street characteristics, as detailed in Lugon et al. (2020). To analyze streets with different characteristics, this section focus on the comparison between the one-way and two-way coupling approaches over the whole street network. As in Lugon et al. (2020), two factors are analyzed to investigate the influence of the two-way coupling on the local-scale concentrations: (i) the strength of traffic

emissions, and (ii) the street aspect ratio α_r (ratio between street height and width). The vertical mass flux between the local and regional scales is proportional to the concentration gradient between the street and the urban background, as shown in Equation (8) of Lugon et al. (2020). Streets with high traffic emissions tend to favor the vertical mass transfer from the local to the regional scales, as they tend to present a high gradient between the street and the urban background concentrations. This vertical mass flux is also dependent of the street geometry, represented by the aspect ratio α_r (see Equation 9 in Lugon et al. (2020)). Streets with low aspect ratio (large streets) tend to favor the vertical transfer between local and regional scales, and in streets with high aspect ratios (narrow streets) the vertical mass transfer between scales tends to be lower. Streets are classified as large streets when $\alpha_r \leq 0.3$, intermediate streets when $0.3 < \alpha_r < 0.6$, and narrow streets when $\alpha_r \geq 0.6$ (Kim et al., 2018).

Figures 6 illustrates, respectively, the average BC emissions in the street network (panel (a)), the average BC concentrations simulated by SinG (panel (b)), the absolute difference between the BC concentrations simulated by SinG and MUNICH (panel (c)), and the absolute relative differences between the BC concentrations simulated by SinG and MUNICH (panel (d)). A good correlation between traffic emissions and concentrations is observed, as expected. The differences between the average BC concentrations simulated by SinG and MUNICH range from -2.6 μg.m^{-3} to 2.4 μg.m^{-3}, corresponding to relative errors between 0% and 50%. The BC concentrations simulated by SinG are higher than those simulated by MUNICH especially in the streets located in the left side of the street network, where the traffic emissions are the highest. This effect is also observed in the streets adjacent to the high-emission streets, probably due to transport of pollutants from one street to another. Even though the BC concentrations are higher in SinG than in MUNICH near streets with high traffic emissions, they are lower in a large part of the domain, in the middle of the street network. This region presents simultaneously low BC emissions and concentrations, and high aspect ratios α_r. Therefore, the concentration gradients between the local and regional scales are low, leading to low differences between local and regional-scale concentrations. However, the absolute values of the relative differences between the concentrations simulated by MUNICH and SinG in this region are large and reach 50%. These large differences and the lower concentrations simulated in SinG compared to MUNICH may be explained by the double counting of traffic emissions performed by MUNICH with the one-way coupling technique. Using the two-way coupling approach in SinG, the streets with low traffic emissions and high aspect ratios present low vertical mass transfer between streets and urban background. This mass transfer is lower than the traffic emissions considered at the regional scale in the one-way coupling approach (MUNICH). This results in lower background concentrations above the streets using the two-way coupling approach (SinG), leading then to lower street concentrations.

In order to evaluate more precisely the influence of the street geometry (represented by α_r) in the relative differences between the BC concentrations simulated by SinG and MUNICH, the analysis of different α_r intervals is made. Figure 7 illustrates the percentage of streets present in different ranges of α_r intervals encountered in the street network for different ranges of relative differences between the BC concentrations simulated by SinG and MUNICH. The sum of each column corresponds to 100%. The streets with low values of α_r (large streets) tend to have more cars passing and higher emission rates. In this case, the BC concentrations tend to be higher using SinG than using MUNICH, and the relative differences are mostly positives. The higher the street aspect ratio α_r is, the higher the percentages of streets with negative relative differences between SinG and MUNICH
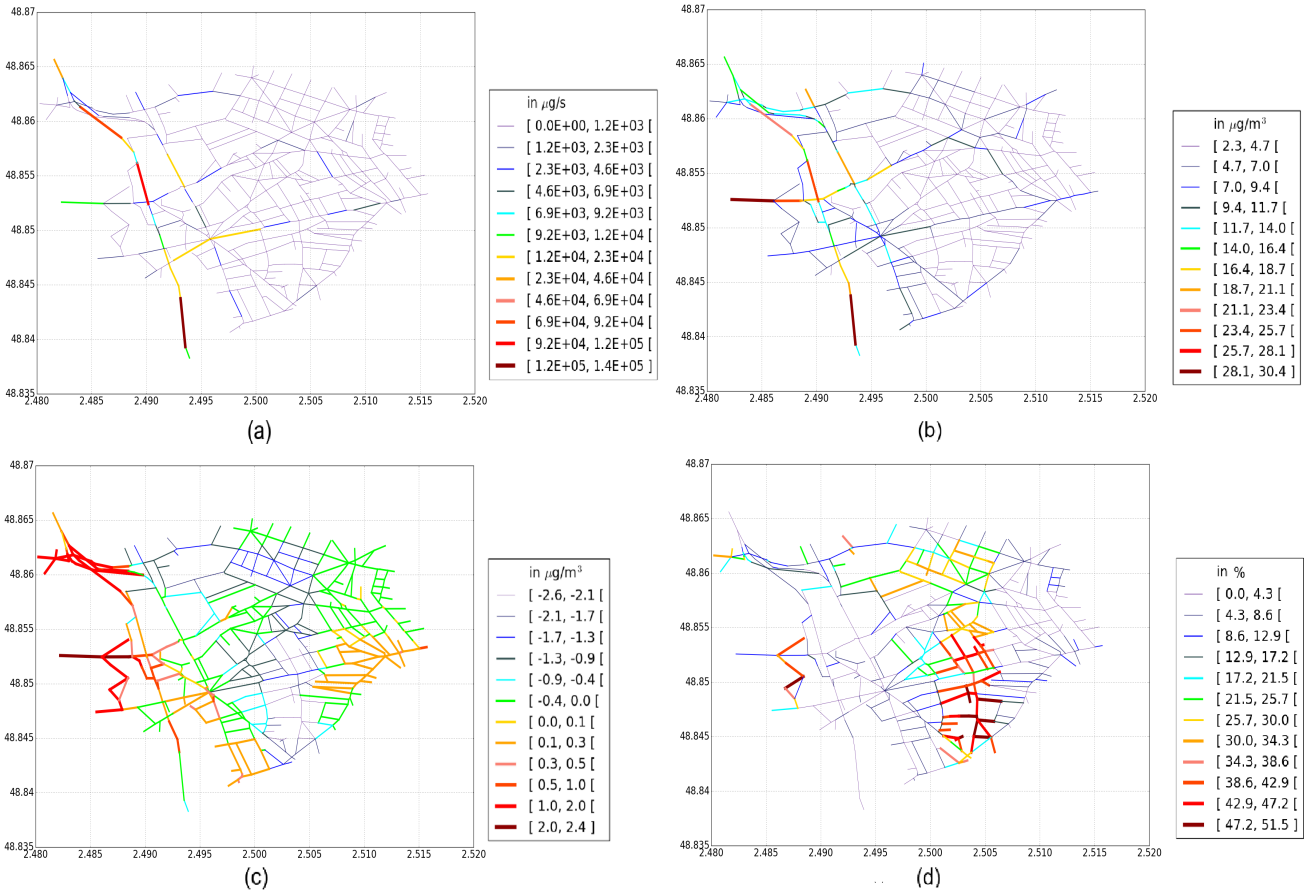
Figure 6. Average BC emissions in the street-network (a), average BC concentrations simulated by SinG (b), absolute differences between the BC concentrations simulated by SinG and MUNICH (c), and absolute values of relative differences between the BC concentrations simulated by SinG and MUNICH (d).

are. The impact of the two-way coupling on BC concentrations in streets is high, with relative differences ranging from -51% to 48%.

7 Conclusion

This study performs simulations of BC concentrations in a Parisian suburb street-network using the multi-scale model SinG. Two main aspects influencing the BC concentrations in streets are investigated: (i) the non-exhaust emissions (tyre, brake and road wear) and particle resuspension; and (ii) the two-way coupling between the street-network model and chemistry transport model that computes the urban background concentrations. A sensitivity analysis on black carbon non-exhaust emissions
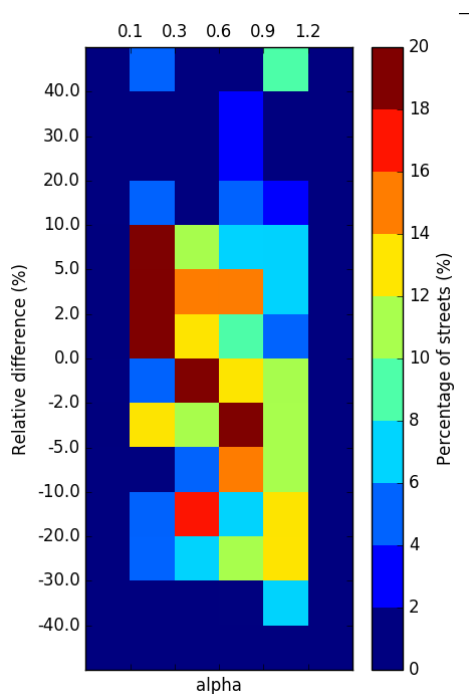
Figure 7. Percentage of streets (purple) present in different α_r intervals for different ranges of the relative differences between the BC concentrations simulated by SinG and MUNICH.

is performed, regarding particularly tyre-wear emissions. A new parametrization to calculate particle resuspension is also presented, respecting the mass balance at the street surface.

Constant resuspension emission factors are often used in the literature to model resuspension, without taking into account the amount of deposited mass. Particle resuspension is not an important source of BC in the simulations here, because the

540 deposited mass over the street surface is not significant enough to justify high constant resuspension emission factors. As the simulated deposited mass agrees well with in-situ measurements, other sources of BC emissions are investigated here. In particular, non-exhaust emissions, such as tyre wear, can be relevant to improve the modelling of BC concentrations in streets. They can be as relevant as exhaust emissions, and their underestimation may justify the virtual increase of BC emissions often employed in street-network modelling studies. This can have direct consequences on public policies aiming at reducing BC

545 concentrations in urban areas: non-exhaust emissions may contribute to as much as half of the BC concentrations in streets.

Non-exhaust emissions still present very high uncertainties, with a large spectrum of emission factors and experimental limitations to separate each non-exhaust emission source. More studies are needed to better characterize these emissions, regarding their size distributions and chemical compositions. In particular, large differences are observed in the literature, between different studies estimating tyre-wear emissions, with tyre-wear emission factors from the EMEP guidelines being

550 on the low side of factors. Following the literature, increasing the BC passenger cars tyre-wear emission factors of the EMEP

guidelines from 1.36 mg.(veh-km)−1 to 20.8 mg.(veh-km)−1 lead to good comparisons of the simulated BC concentrations to the measured ones. The authors highlight that additional work, mostly experimental, should be conducted to confirm this result. Also, more studies are needed to control these emissions. Some studies already indicate the importance of controlling vehicle speed and/or smoothing traffic flow to reduce non-exhaust emissions (Beji et al., 2020). But other aspects can be investigated, such as the road, tyre and brake characteristics, vehicle weight, etc. However, the work presented here makes a very strong case for revising current BC vehicular emission inventories and taking non-exhaust emissions explicitly into account in air quality simulations.

The two-way coupling rather than one-way coupling between the local and regional scales proved to strongly influence the BC concentrations in streets. This is because the BC concentration gradients observed between the streets (local-scale) and the urban background (regional-scale) are often high. The intensity of the vertical mass flux between streets and background are function of traffic emissions and street geometry (represented by the aspect ratio α_r). The two-way coupling leads to higher BC concentrations in large streets with high traffic emissions, and lower BC concentrations in narrow streets with low traffic emissions (with differences ranging from -51.5% to 48.4%).

Appendix A: Statistical parameters

A1   Definitions

- FB: Fractional bias
$$FB = 2\left(\frac{\bar{o}-\bar{c}}{\bar{o}+\bar{c}}\right)$$

- MG: Geometric mean bias
$$MG = exp(\overline{ln(o)} - \overline{ln(c)})$$

- NMSE: Normalized mean square error
$$NMSE = \frac{\overline{(o-c)^2}}{\bar{o}\bar{c}}$$

- VG: Geometric variance
$$VG = exp[\overline{(ln(o) - ln(c))^2}]$$

- NAD: Normalised absolute difference
$$NAD = \frac{\overline{|c-o|}}{(\bar{c}+\bar{o})}$$

- FAC2: Fraction of data that satisfy
$$0.5 \leq \frac{c}{o} \leq 2.0$$

Where o and c represent the observed and simulated concentrations respectively.

A2   Statistical indicators obtained with SinG and MUNICH-only simulations at "Boulevard Alsace-Lorraine"

Table A1. Comparisons to BC measurements at "Boulevard Alsace-Lorraine": statistical indicators obtained with SinG and MUNICH-only simulations.

	o [μg.m^{-3}]	s [μg.m^{-3}]	FB	MG	NMSE	VG	FAC2	NAD
SinG	6.07	4.91	-0.21	0.82	0.29	1.27	0.77	0.19
MUNICH-only	6.07	4.97	-0.19	0.82	0.33	1.32	0.74	0.20

A3 Details of the particle size distribution from non-exhaust emissions

Table A2. Size distribution of the total suspended particles emitted from non-exhaust emissions used in the simulations, with the coarse PM fraction ($f_s^{pm2.5-10}$), PM$_{2.5}$ fraction ($f_s^{pm2.5}$) and PM$_1$ fraction (f_s^{pm1}) adopted in each wear emission source (tyre wear indicated by ty, brake wear indicated by bk, and road wear indicated by rd).

Sim.	$f_{ty}^{pm2.5-10}$	$f_{ty}^{pm2.5}$	f_{ty}^{pm1}	$f_{bk}^{pm2.5-10}$	$f_{bk}^{pm2.5}$	f_{bk}^{pm1}	$f_{rd}^{pm2.5-10}$	$f_{rd}^{pm2.5}$	f_{rd}^{pm1}	Reference
1[3]	-	-	-	-	-	-	-	-	-	-
2[4]	0.18	0.42	0.06	0.59	0.39	0.10	0.23	0.27	n/a[5]	Ntziachristos and Boulter (2016)
3	0.09	0.01	n/a	0.30	0.50	n/a	0.172	0.008	n/a	Denby et al. (2013a)

Author contributions. KS and LL were responsible for conceptualization. LL developed the software. LL conduced the visualization and validation; LL and KS performed the formal analysis. JV, KS and CD acquired resources. KS and OC were responsible for funding acquisition. LL and KS were responsible for writing and original draft preparation.

Competing interests. The authors declare that they have no conflict of interest.

Data availability. The source code of Street-in-Grid and MUNICH models are available via Zenodo with the following DOI https://doi.org/10.5281/zenodo.4393638. The observation data are available from AIRPARIF, Air quality – TRAFIPOLLU campaing. They are available upon request.

[5]Only exhaust emissions are considered (Ntziachristos and Samaras, 2018).
[5]Same size distribution used in simulations 4, 5 and 6.
[5]n/a: not available in the reference.

Acknowledgements. This research has been supported by the Department of Green Spaces and Environment (Mairie de Paris) and the École des Ponts ParisTech (grant CIFRE no. 2017/064). The authors thank Airparif for providing the emission inventory and the measured concentration data, and the TRAFIPOLLU ANR project for making data available for the model application and evaluation.

590

References

Abu-Allaban, M., Gillies, J. A., Gertler, A. W., Clayton, R., and Proffitt, D.: Tailpipe, resuspended road dust, and brake-wear emission factors from on-road vehicles, Atmos. Environ., 37, 5283–5293, https://doi.org/10.1016/j.atmosenv.2003.05.005, 2003.

AIRPARIF: Source apportionment of airbone particles in the Île-de-France region, Tech. rep., Air-quality agency of Paris, https://www.airparif.asso.fr/_pdf/publications/rapport-particules-anglais-120829.pdf, 2012.

Amato, F., Pandolfi, M., Viana, M., Querol, X., Alastuey, A., and Moreno, T.: Spatial and chemical patterns of PM_{10} in road dust deposited in urban environment, Atmos. Environ., 43, 1650–1659, https://doi.org/10.1016/j.atmosenv.2008.12.009, 2009.

Awad, Y. A., Koutrakis, P., Coull, B. A., and Schwartz, J.: A spatio-temporal prediction model based on support vector machine regression: ambient black carbon in three New England states, Environ. Res., 159, 427–434, https://doi.org/10.1016/j.envres.2017.08.039, 2017.

Baekken, T.: Environmental effects of asphalt and tyre wear by road traffic, Tech. rep., Nordisk Seminor-og Arbejdsrapporter 1993, 1993.

Baumann, W. and Ismeier, M.: Exemplarische Erfassung der Umweltexposition ausgewählter Kauschukderivate bei der bestimmungsgemäßen Verwendung in Reifen und deren Entsorgung, Endbericht zum Forschungsvorhaben, 206, 081, 1997.

Beji, A., Deboudt, K., Khardi, S., Muresan, B., Flament, P., Fourmentin, M., and Lumière, L.: Non-exhaust particle emissions under various driving conditions: Implications for sustainable mobility, Transp. Res. Part D, 81, 102 290, https://doi.org/10.1016/j.trd.2020.102290, 2020.

Berdowski, J., Visschedijk, A., Creemers, E., and Pulles, T.: The coordinated European programme on particulate matter emission inventories, projections and guidance (CEPMEIP) Database. TNO-MEP, Apeldoorn, NL, Tech. rep., TNO-MEP, Apeldoorn, NL, Online-Version under: www.air.sk/tno/cepmeip, 2002.

Boniardi, L., Dons, E., Campo, L., Van Poppel, M., Panis, L. I., and Fustinoni, S.: Annual, seasonal, and morning rush hour land use regression models for black carbon in a school catchment area of Milan, Italy, Environ. Res., https://doi.org/10.1016/j.envres.2019.06.001, 2019.

Boulter, P.: A review of emission factors and models for road vehicle non-exhaust particulate matter, Tech. rep., TRL Limited, Wokingham, UK.(TRL Report PPR065), 2005.

Boutahar, J., Lacour, S., Mallet, V., Quélo, D., Roustan, Y., and Sportisse, B.: Development and validation of a fully modular platform for numerical modelling of air pollution: POLAIR, Int. J. Environ. Pollut., 22, 17–28, https://doi.org/10.1504/IJEP.2004.005474, 2004.

Brasseur, O., Declerck, P., Heene, B., and Vanderstraeten, P.: Modelling Black Carbon concentrations in two busy street canyons in Brussels using CANSBC, Atmos. Environ., 101, 72–81, https://doi.org/10.1016/j.atmosenv.2014.10.049, 2015.

Chen, Y., Schleicher, N., Fricker, M., Cen, K., Liu, X.-l., Kaminski, U., Yu, Y., Wu, X.-f., and Norra, S.: Long-term variation of black carbon and $PM_{2.5}$ in Beijing, China with respect to meteorological conditions and governmental measures, Environ. Pollut., 212, 269–278, https://doi.org/10.1016/j.envpol.2016.01.008, 2016.

Cherin, N., Roustan, Y., Musson-Genon, L., and Seigneur, C.: Modelling atmospheric dry deposition in urban areas using an urban canopy approach, Geosci. Model Dev., 8, 893, https://doi.org/10.5194/gmd-8-893-2015, 2015.

Chung, S. H. and Seinfeld, J. H.: Climate response of direct radiative forcing of anthropogenic black carbon, J. Geophys. Res., 110, https://doi.org/10.1029/2004JD005441, 2005.

Councell, T. B., Duckenfield, K. U., Landa, E. R., and Callender, E.: Tire-wear particles as a source of zinc to the environment, Environ. Sci. Technol., 38, 4206–4214, https://doi.org/10.1021/es034631f, 2004.

de Miranda, R. M., Perez-Martinez, P. J., de Fatima Andrade, M., and Ribeiro, F. N. D.: Relationship between black carbon (BC) and heavy traffic in São Paulo, Brazil, Transp. Res. Part D, 68, 84–98, https://doi.org/10.1016/j.trd.2017.09.002, 2019.

Denby, B. R., Sundvor, I., Johansson, C., Pirjola, L., Ketzel, M., Norman, M., Kupiainen, K., Gustafsson, M., Blomqvist, G., and Omstedt, G.: A coupled road dust and surface moisture model to predict non-exhaust road traffic induced particle emissions (NORTRIP). Part 1: Road dust loading and suspension modelling, Atmos. Environ., 77, 283–300, https://doi.org/10.1016/j.atmosenv.2013.04.069, 2013a.

Denby, B. R., Sundvor, I., Johansson, C., Pirjola, L., Ketzel, M., Norman, M., Kupiainen, K., Gustafsson, M., Blomqvist, G., and Omstedt, G.: A coupled road dust and surface moisture model to predict non-exhaust road traffic induced particle emissions (NORTRIP). Part 2: Surface moisture and salt impact modelling, Atmos. Environ., 81, 485–503, https://doi.org/10.1016/j.atmosenv.2013.09.003, 2013b.

Dons, E., Panis, L. I., Van Poppel, M., Theunis, J., and Wets, G.: Personal exposure to black carbon in transport microenvironments, Atmos. Environ., 55, 392–398, https://doi.org/10.1016/j.atmosenv.2012.03.020, 2012.

Dore, C. J., Goodwin, J. W. L., Watterson, J. D., Murrells, T. P., Passant, N. R., Hobson, M. M., Haigh, K. E., Baggott, S. L., Pye, S. T., Coleman, P. J., and King, K. R.: UK emissions of air pollutants 1970 to 2001, National Atmospheric Emissions Inventory, 2003.

Gebbe, H.: Quantifizierung des reifenabriebs von kraftfahrzeugen in Berlin, ISS-Fahrzeugtechnik, TU Berlin, im Auftrag der Senatsverwaltung für Stadtentwicklung, Umweltschutz und Technologie Berlin, 1997.

Grigoratos, T. and Martini, G.: Brake wear particle emissions: a review, Environ. Sci. Pollut. Res., 22, 2491–2504, https://doi.org/10.1007/s11356-014-3696-8, 2015.

Guevara, M., Tena, C., Porquet, M., Jorba, O., and Pérez García-Pando, C.: HERMESv3, a stand-alone multi-scale atmospheric emission modelling framework–Part 2: The bottom–up module, Geosci. Model Dev., 13, 873–903, 2020.

Hanna, S. and Chang, J.: Acceptance criteria for urban dispersion model evaluation, Meteorol. Atmos. Phys., 116, 133–146, https://doi.org/10.1007/s00703-011-0177-1, 2012.

Harrison, R. M., Yin, J., Mark, D., Stedman, J., Appleby, R. S., Booker, J., and Moorcroft, S.: Studies of the coarse particle (2.5–10 μm) component in UK urban atmospheres, Atmos. Environ., 35, 3667–3679, https://doi.org/10.1016/S1352-2310(00)00526-4, 2001.

Herring, S. and Huq, P.: A review of methodology for evaluating the performance of atmospheric transport and dispersion models and suggested protocol for providing more informative results, Fluids, 3, 20, https://doi.org/10.3390/fluids3010020, 2018.

Highwood, E. J. and Kinnersley, R. P.: When smoke gets in our eyes: The multiple impacts of atmospheric black carbon on climate, air quality and health, Environ. Int., 32, 560–566, https://doi.org/10.1016/j.envint.2005.12.003, 2006.

Hong, Y., Bonhomme, C., Le, M.-H., and Chebbo, G.: A new approach of monitoring and physically-based modelling to investigate urban wash-off process on a road catchment near Paris, Water Res., 102, 96–108, https://doi.org/10.1016/j.watres.2016.06.027, 2016a.

Hong, Y., Bonhomme, C., Le, M.-H., and Chebbo, G.: New insights into the urban washoff process with detailed physical modelling, Sci. Total Environ., 573, 924–936, https://doi.org/10.1016/j.scitotenv.2016.08.193, 2016b.

Invernizzi, G., Ruprecht, A., Mazza, R., De Marco, C., Močnik, G., Sioutas, C., and Westerdahl, D.: Measurement of black carbon concentration as an indicator of air quality benefits of traffic restriction policies within the ecopass zone in Milan, Italy, Atmos. Environ., 45, 3522–3527, https://doi.org/10.1016/j.atmosenv.2011.04.008, 2011.

Jacobson, M. Z.: Strong radiative heating due to the mixing state of black carbon in atmospheric aerosols, Nature, 409, 695, https://doi.org/10.1038/35055518, 2001.

Jansen, K. L., Larson, T. V., Koenig, J. Q., Mar, T. F., Fields, C., Stewart, J., and Lippmann, M.: Associations between health effects and particulate matter and black carbon in subjects with respiratory disease, Environ. Health Perspect., 113, 1741–1746, https://doi.org/10.1289/ehp.8153, 2005.

Janssen, N. A. H., Hoek, G., Simic-Lawson, M., Fischer, P., Van Bree, L., Ten Brink, H., Keuken, M., Atkinson, R. W., Anderson, H. R., Brunekreef, B., and Casse, F. R.: Black carbon as an additional indicator of the adverse health effects of airborne particles compared with PM_{10} and $PM_{2.5}$, Environ. Health Perspect., 119, 1691–1699, https://doi.org/10.1289/ehp.1003369, 2011.

Jones, R. R., Hoek, G., Fisher, J. A., Hasheminassab, S., Wang, D., Ward, M. H., Sioutas, C., Vermeulen, R., and Silverman, D. T.: Land use regression models for ultrafine particles, fine particles, and black carbon in southern California, Sci. Total Environ., 699, 134 234, https://doi.org/10.1016/j.scitotenv.2019.134234, 2020.

Khare, P., Machesky, J., Soto, R., He, M., Presto, A. A., and Gentner, D. R.: Asphalt-related emissions are a major missing nontraditional source of secondary organic aerosol precursors, Sci. Adv., 6, eabb9785, https://doi.org/10.1126/sciadv.abb9785, 2020.

Kim, Y., Wu, Y., Seigneur, C., and Roustan, Y.: Multi-scale modeling of urban air pollution: development and application of a Street-in-Grid model (v1. 0) by coupling MUNICH (v1. 0) and Polair3D (v1. 8.1), Geosci. Model Dev., 11, 611, https://doi.org/10.5194/gmd-11-611-2018, 2018.

Kreider, M. L., Panko, J. M., McAtee, B. L., Sweet, L. I., and Finley, B. L.: Physical and chemical characterization of tire-related particles: Comparison of particles generated using different methodologies, Sci. Total Environ., 408, 652–659, 2010.

Lawrence, S., Sokhi, R., and Ravindra, K.: Quantification of vehicle fleet PM_{10} particulate matter emission factors from exhaust and non-exhaust sources using tunnel measurement techniques, Environ. Pollut., 210, 419–428, https://doi.org/10.1016/j.envpol.2016.01.011, 2016.

Lequy, E., Siemiatycki, J., de Hoogh, K., Vienneau, D., Dupuy, J.-F., Garès, V., Hertel, O., Christensen, J. H., Zhivin, S., Goldberg, M., et al.: Contribution of Long-Term Exposure to Outdoor Black Carbon to the Carcinogenicity of Air Pollution: Evidence regarding Risk of Cancer in the Gazel Cohort, Environmental health perspectives, 129, 037 005, 2021.

Li, X., Huang, L., Li, J., Shi, Z., Wang, Y., Zhang, H., Ying, Q., Yu, X., Liao, H., and Hu, J.: Source contributions to poor atmospheric visibility in China, Resour. Conserv. Recycl., 143, 167–177, https://doi.org/10.1016/j.resconrec.2018.12.029, 2019.

Liu, M., Peng, X., Meng, Z., Zhou, T., Long, L., and She, Q.: Spatial characteristics and determinants of in-traffic black carbon in Shanghai, China: Combination of mobile monitoring and land use regression model, Sci. Total Environ., 658, 51–61, https://doi.org/10.1016/j.scitotenv.2018.12.135, 2019.

Lugon, L., Sartelet, K., Kim, Y., Vigneron, J., and Chrétien, O.: Nonstationary modeling of NO_2, NO and NO_x in Paris using the Street-in-Grid model: coupling local and regional scales with a two-way dynamic approach, Atmos. Chem. Phys., 20, 7717–7740, https://doi.org/10.5194/acp-20-7717-2020, 2020.

Luhana, L., Sokhi, R., Warner, L., Mao, H., Boulter, P., McCrae, I., Wright, J., and Osborn, D.: Measurement of non-exhaust particulate matter. Characterisation of exhaust particulate emissions from road vehicles (PARTICULATES). Deliverable, Tech. rep., https://ec.europa.eu/transport/road_safety/sites/roadsafety/files/pdf/projects_sources/particulates_d8.pdf, 2004.

Lyu, Y. and Olofsson, U.: On black carbon emission from automotive disc brakes, J. Aero. Sci., p. 105610, https://doi.org/10.1016/j.jaerosci.2020.105610, 2020.

Majdi, M., Kim, Y., Turquety, S., and Sartelet, K.: Impact of mixing state on aerosol optical properties during severe wildfires over the Euro-Mediterranean region, Atmos. Environ., 220, 117 042, https://doi.org/10.1016/j.atmosenv.2019.117042, 2020.

Mallet, V., Quélo, D., Sportisse, B., Ahmed De Biasi, M., Debry, E., Korsakissok, I., Wu, L., Roustan, Y., Sartelet, K., Tombette, M., and Foudhil, H.: Technical Note: The air quality modeling system Polyphemus, Atmos. Chem. Phys., 7, 6459–6486, https://hal.archives-ouvertes.fr/hal-00328079, 2007.

Malmqvist, P.-A.: Urban stormwater pollutant sources-an analysis of inflows and outflows of nitrogen, phosphorus, lead, zinc and copper in urban areas, Chalmers University of Technology, 1983.

Moosmüller, H., Gillies, J., Rogers, C., DuBois, D., Chow, J., Watson, J., and Langston, R.: Particulate emission rates for unpaved shoulders along a paved road, J. Air. & Waste Manage. Assoc., 48, 398–407, https://doi.org/10.1080/10473289.1998.10463694, 1998.

705 Ntziachristos, L. and Boulter, P.: 1.A.3.b.vi Road transport: Automobile tyre and brake wear; 1.A.3.b.vii Road tranport: Automobile road abrasion, European Environment Agency (EEA): EMEP/EEA air pollutant emission inventory guidebook 2016, https://www.eea.europa.eu/publications/emep-eea-guidebook-2016/part-b-sectoral-guidance-chapters/1-energy/1-a-3-b-vi, 2016.

Ntziachristos, L. and Samaras, Z.: EMEP/EEA—Air Pollutant Emission Inventory Guidebook 2016—Update Jul. 2018, European Environment Agency: Copenhagen, Denmark, https://www.eea.europa.eu/publications/emep-eea-guidebook-2016/
710 part-b-sectoral-guidance-chapters/1-energy/1-a-3-b-i, 2018.

Park, I., Lee, J., and Lee, S.: Laboratory study of the generation of nanoparticles from tire tread, Aerosol Sci. Tech., 51, 188–197, https://doi.org/10.1080/02786826.2016.1248757, 2017.

Park, I., Kim, H., and Lee, S.: Characteristics of tire wear particles generated in a laboratory simulation of tire/road contact conditions, J. Aero. Sci., 124, 30–40, https://doi.org/10.1016/j.jaerosci.2018.07.005, 2018.

715 Pay, M. T., Jiménez-Guerrero, P., and Baldasano, J. M.: Implementation of resuspension from paved roads for the improvement of CALIOPE air quality system in Spain, Atmos. Environ., 45, 802–807, https://doi.org/10.1016/j.atmosenv.2010.10.032, 2011.

Ramachandran, S. and Kedia, S.: Black carbon aerosols over an urban region: radiative forcing and climate impact, J. Geophys. Res., 115, https://doi.org/10.1029/2009JD013560, 2010.

Rauterberg-Wulff, A.: Determination of emission factors for tire wear particles by tunnel measurements, in: 8th International Symposium"
720 Transport and Air Pollution", June 1999 Graz, Austria, 1999.

Richmond-Bryant, J., Saganich, C., Bukiewicz, L., and Kalin, R.: Associations of $PM_{2.5}$ and black carbon concentrations with traffic, idling, background pollution, and meteorology during school dismissals, Sci. Total Environ., 407, 3357–3364, https://doi.org/10.1016/j.scitotenv.2009.01.046, 2009.

Sanchez, M., Ambros, A., Milà, C., Salmon, M., Balakrishnan, K., Sambandam, S., Sreekanth, V., Marshall, J. D., and Tonne, C.: Devel-
725 opment of land-use regression models for fine particles and black carbon in peri-urban South India, Sci. Total Environ., 634, 77–86, https://doi.org/10.1016/j.scitotenv.2018.03.308, 2018.

Sanders, P. G., Xu, N., Dalka, T. M., and Maricq, M. M.: Airborne brake wear debris: size distributions, composition, and a comparison of dynamometer and vehicle tests, Environ. Sci. Technol., 37, 4060–4069, https://doi.org/10.1021/es034145s, 2003.

Sartelet, K., Debry, E., Fahey, K., Roustan, Y., Tombette, M., and Sportisse, B.: Simulation of aerosols and gas-phase species
730 over Europe with the POLYPHEMUS system: Part I—Model-to-data comparison for 2001, Atmos. Environ., 41, 6116–6131, https://doi.org/10.1016/j.atmosenv.2007.04.024, 2007.

Schuring, D. and Clark, J.: Load, speed, and pressure effects on passenger car tire rolling-loss distribution, Rubber Chem. Technol., 61, 669–687, https://doi.org/10.5254/1.3536212, 1988.

Tao, J., Ho, K.-F., Chen, L., Zhu, L., Han, J., and Xu, Z.: Effect of chemical composition of $PM_{2.5}$ on visibility in Guangzhou, China, 2007
735 spring, Particuology, 7, 68–75, https://doi.org/10.1016/j.partic.2008.11.002, 2009.

Thorpe, A. and Harrison, R. M.: Sources and properties of non-exhaust particulate matter from road traffic: a review, Sci. Total Environ., 400, 270–282, https://doi.org/10.1016/j.scitotenv.2008.06.007, 2008.

Thorpe, A. J., Harrison, R. M., Boulter, P. G., and McCrae, I. S.: Estimation of particle resuspension source strength on a major London Road, Atmos. Environ., 41, 8007–8020, https://doi.org/10.1016/j.atmosenv.2007.07.006, 2007.

740 Thouron, L., Seigneur, C., Kim, Y., Mahé, F., André, M., Bruge, B., Chanut, H., and Pellan, Y.: Intercomparison of three modeling approaches for traffic-related road dust resuspension using two experimental data, Transp. Res. Part D, 58, 108–121, https://doi.org/10.1016/j.trd.2017.11.003, 2018.

Tong, Z., Wang, Y. J., Patel, M., Kinney, P., Chrillrud, S., and Zhang, K. M.: Modeling spatial variations of black carbon particles in an urban highway-building environment, Environ. Sci. Technol., 46, 312–319, https://doi.org/10.1021/es201938v, 2011.

745 Tripathi, S., Dey, S., Tare, V., and Satheesh, S.: Aerosol black carbon radiative forcing at an industrial city in northern India, Geophys. Res. Lett., 32, https://doi.org/10.1029/2005GL022515, 2005.

Van den Bossche, J., De Baets, B., Verwaeren, J., Botteldooren, D., and Theunis, J.: Development and evaluation of land use regression models for black carbon based on bicycle and pedestrian measurements in the urban environment, Environ. Modell. Softw., 99, 58–69, https://doi.org/10.1016/j.envsoft.2017.09.019, 2018.

750 Van den Hove, A., Verwaeren, J., Van den Bossche, J., Theunis, J., and De Baets, B.: Development of a land use regression model for black carbon using mobile monitoring data and its application to pollution-avoiding routing, Environ. Res., p. 108619, https://doi.org/10.1016/j.envres.2019.108619, 2019.

Vaze, J. and Chiew, F. H.: Experimental study of pollutant accumulation on an urban road surface, Urban Water, 4, 379–389, https://doi.org/10.1016/S1462-0758(02)00027-4, 2002.

755 Venkatram, A., Fitz, D., Bumiller, K., Du, S., Boeck, M., and Ganguly, C.: Using a dispersion model to estimate emission rates of particulate matter from paved roads, Atmos. Environ., 33, 1093–1102, https://doi.org/10.1016/S1352-2310(98)00316-1, 1999.

Zhang, L., Cheng, S., Jiang, X., Zhang, J., Meng, P., Tang, Q., Qin, X., Wang, B., Chen, C., and Zou, Z.: Pregnancy exposure to carbon black nanoparticles exacerbates bleomycin-induced lung fibrosis in offspring via disrupting LKB1-AMPK-ULK1 axis-mediated autophagy, Toxicology, 425, 152 244, https://doi.org/10.1016/j.tox.2019.152244, 2019a.

760 Zhang, Y., Tu, B., Jiang, X., Xu, G., Liu, X., Tang, Q., Bai, L., Meng, P., Zhang, L., Qin, X., et al.: Exposure to carbon black nanoparticles during pregnancy persistently damages the cerebrovascular function in female mice, Toxicology, 422, 44–52, https://doi.org/10.1016/j.tox.2019.04.014, 2019b.

Zhu, S., Sartelet, K., Zhang, Y., and Nenes, A.: Three-dimensional modeling of the mixing state of particles over Greater Paris, J. Geophys. Res., 121, 5930–5947, https://doi.org/10.1002/2015JD024241, 2016.